32ND INTERNATIONAL COSMIC RAY CONFERENCE, BEIJING 2011

Cosmic ray elemental composition study by using an artificial neural network based on the measurement of the lateral particle density distribution in showers induced by primaries in the 30-10000 TeV energy region

A. CIRILLO[1,2], S. M. MARI[1,2], P. MONTINI[1,2]
[1] *Università degli Studi "Roma TRE" - Dipartimento di Fisica*
[2] *INFN - Sezione di Roma TRE*
mari@fis.uniroma3.it

DOI: 10.7529/ICRC2011/V01/0691

Abstract: The mass composition plays an important role for understanding the origin of the UHE cosmic rays. The composition in the energy region at and beyond the knee is important because it is related to the sites of cosmic ray productions and accelerations. In order to perform the composition measurement, an artificial neural network (ANN) has been implemented, it is based on a set of composition estimators obtained by a detailed study of the lateral particle density distribution. Showers induced by protons, He nuclei, CNO group and iron nuclei have been generated in the energy region (30-10000) TeV, the lateral particle density distribution was estimated. In this paper the estimators are presented, the performance of the mass discrimination is discussed.

Keywords: Cosmic Rays, Composition, Neural Network

1 Introduction

The study of the mass composition of high energy cosmic rays can provide important informations about their origin, acceleration and propagation mechanisms. Cosmic rays at energies below the knee are of galactic origin and are accelerated in the galactic supernova remnants. In the higher energy region of the spectrum there are no galactic sources capable to accelerate particles up to these energies. A change of the elemental composition at the knee could be an indication of the transition between galactic and extra–galactic cosmic rays. Moreover the composition of the cosmic rays at the energy of the knee is connected to the source abundance and to the acceleration mechanisms, cosmic rays generated by supernova remnants and accelerated at shocks are expected to be iron-enriched as the energy increases. At these high energies the extra–galactic cosmic rays are expected to be dominated by light elements because of the spallation processes. At energies below 100 TeV the mass composition can be directly measured with satellite or balloon–borne detectors. At energies greater than 100 TeV the mass composition must be measured by means of indirect technique. This technique involves the detection of extensive air showers produced by the interaction of the primary particles with Earth's atmosphere. Although the estimation of the energy and of the direction of cosmic rays from EAS data is relatively easy, the estimation of the identity of the primary is a very difficult task. Showers produced by different primaries present differences that are covered by the variation of the primary energy, by the uncertainties in hadronic interaction models and by fluctuations of the showers.
In this work a mass composition discrimination is presented based on a detailed measurement of the particle distribution of the shower front in EAS events. The Monte Carlo events have been sampled by means of an ideal, fine-segmented, full-coverage detector. The lateral particle distribution has been characterized by eight parameters, described in section 4, which have been used to distinguish the primary particle type of cosmic rays [2]. In this work we present a study of the elemental composition of cosmic rays by using the lateral particle distribution.

2 The Monte Carlo data sample

A large Monte Carlo data sample has been generated for this analysis by using the CORSIKA (v. 6.90) code, including QGSJET-II and FLUKA [1] hadronic interaction models. Showers produced by protons, Helium nuclei, CNO group and iron nuclei were generated in five energy bins spanning the interval $(31.6 \div 10^4)$ TeV with a power law spectrum according to [3] and in the zenith angle range $(0^\circ \div 45^\circ)$. Showers were sampled at an altitude of about 4000 m a.s.l. In table 3 the numbers of generated events in each energy bin are reported. The showers have been processed by a code simulating an ideal full-coverage pixel-like detector with active elements (scintillators or gaseous detector) of the order of 1 m^2. The ideal detector considered in this work has a total area of about 160×160 m^2

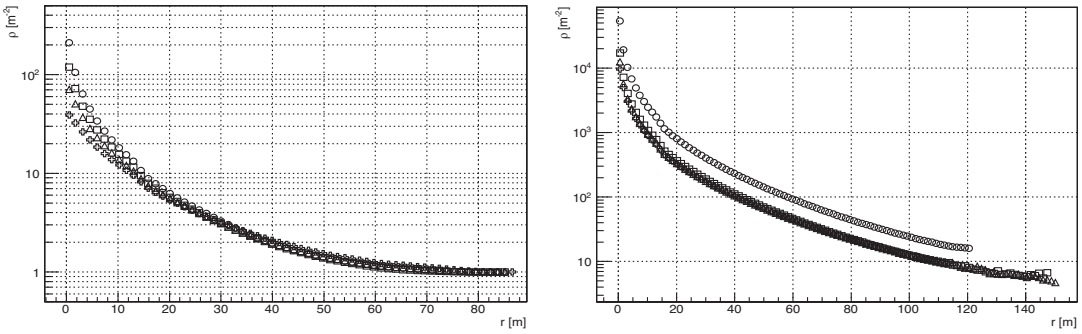

Figure 1: Lateral charged particle density distribution in the multiplicity range M2 (left) and M4 (right). Distributions for protons (circles), helium nuclei (squares), CNO group (triangles) and iron (crosses) are shown.

E [TeV]	p	He	CNO	Fe
31.6–100	100000	28000	28000	28000
100–316	40000	18000	16000	16000
316–1000	20000	8000	8000	8000
1000–3160	2000	1200	1200	1200
3160–10000	800	400	400	400

Table 1: The Monte Carlo data sample used in this analysis

Multiplicity Range	Mean energy [TeV]			
	p	He	CNO	Fe
M_1 $4.7\,10^3 - 2.7\,10^4$	44.9	46.9	49.8	55.3
M_2 $2.7\,10^4 - 2.2\,10^5$	89.9.0	127.8	152.5	218.4
M_3 $2.2\,10^5 - 2.6\,10^6$	617.4	713.2	762.5	965.7
M_4 $2.6\,10^6 - 3.0\,10^7$	8013	6514	7018	7465

Table 2: The multiplicity bins used in this analysis and the corresponding mean energy for each primary type.

with an active area greater than 90%. A simple square geometry has been simulated, a detector efficiency of about 90% has been also considered. A general trigger has been implemented based on a majority logic, events have been recorded with more than 100 hits in a time interval of 1 μs.

3 Data analysis

The core of the simulated showers have been randomly spread on the detector surface, the shower front has been sampled and the charged particles hitting the detector have been recorded. A simple center of mass algorithm has been applied in order to reconstruct the shower core. The events have been selected by applying the following criteria:

1. zenith angle ϑ in the range $(0^\circ - 30^\circ)$
2. reconstructed core position localized in a square of about 120×120 m^2 (75 % of the total area), centered in the detector geometrical center.

The analysis was completed by evaluating the charged particle density $\rho(r)$ as a function of the distance r from the core position, for each primary type and in the four multiplicity bins reported in table 2.

As an example, in figure 1 the particle density distributions $\rho(r)$ are reported for each primary mass in the M_2 and M_4 multiplicity bins. The features of the density distributions obtained in this work allow the determination of a set of parameters which can be used to distinguish different primary masses, as described in the next section.

4 Composition sensitive parameters

The following composition–sensitive parameters have been determined by analyzing the particle density distributions obtained in this analysis:

1. ρ_0: particle density measured in an area of 4 m^2 around the core and centered on the core position
2. β: ratio between the particle density measured at 25 m from the core position (ρ_{25}) and ρ_0
3. $B = \sum_{i=0}^{25} \rho_i/\rho_0$: sum of the values of the ratio ρ_i/ρ_0 up to 25 m from the core position
4. $F(r) = \sum_{pixel} \frac{|N_{hits} - < N_{hits} >|}{\sqrt{< N_{hits} >}}$: sum of the fluctuations of the number of hits detected by each pixel unit, where the mean $< N_{hits} >$ is computed event by event as a function of the distance (r) from the core of the shower,
5. N_{max}: sum of the local maxima,
6. $D_j = u_j D_{r_1} + v_j D_{r_2} + w_j D_{r_3}$: sum of the gradients of the particle density distribution computed at different distances (r_i) from the core,

where

$$D_{r_1} = \frac{2\rho_0 - (\rho_1 + \rho_2)}{2\rho_0}$$

$$D_{r_i} = \frac{(\rho_{i-1} + \rho_i) - (\rho_{i+1} + \rho_{i+2})}{\rho_{i-1} + \rho_i} \qquad i = 2, 3$$

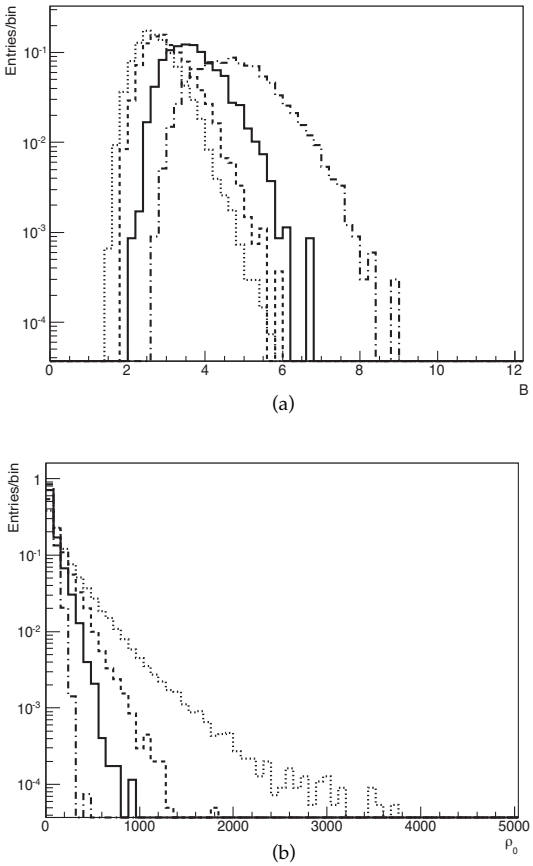

Figure 2: Distributions of the parameter B in the multiplicity range M_3 (a) and of the parameter ρ_0 in the multiplicity range M_2 (b). Values for protons (dotted line), helium (dashed line), CNO (solid line) and iron (dashed–dotted line) are reported.

The distributions of these parameters have been studied as a function of the primary mass in the four multiplicity bins. As an example, the distributions of the B and ρ_0 are reported in figure 2. The plots show the values of the B parameters in the multiplicity bin M_3 (a), and the values of the ρ_0 parameters in the M_2 multiplicity bin (b). These plots show a different shape of the B and ρ_0 parameters which can be used to distinguish showers induced by different primaries. The eight parameters described in the previous section have been used to set up a discrimination function

$$S(\rho, \beta, B, F, N_{max}, D_1, D_2, D_3)$$

by means of a standard two layers perceptron neural network, with the inputs reading the eight parameters for each event. The efficiency of the selection of each primary mass obtained by applying the selection function S are reported in figure 3 for the four multiplicity bins. The contamination for each primary mass, defined by the number of the wrong

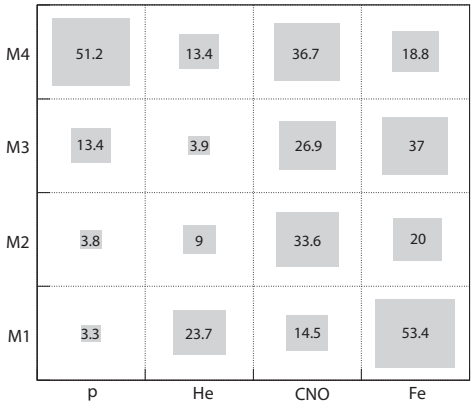

Figure 3: Values of the efficiency (%) of selection obtained by applying the discrimination function S.

primaries selected by the function S, are reported in each row of table 3. The data reported in figure 3 and in table 3 show that at high multiplicities it is possible to discriminate the heavy component with a negligible contamination of the light component.

	p	He	CNO	Fe
p	–	7	2	< 1
He	1	–	2	< 1
CNO	3	18	–	18
Fe	< 1	4	1	–

Table 3: Values of the contamination (%) due to different primary masses

5 Conclusions

In this paper a study of cosmic ray composition in the energy range (30-10000) TeV based on the EAS lateral particle density is reported. An ideal pixel-like detector operating at high altitude was also simulated. A discrimination function was set by means on a standard neural network to separate different primary mass. The function allows the selection of the heavy cosmic ray component with low contamination of light cosmic ray component. As an example in showers with more than $2 \cdot 10^6$ particles, the light component spectrum can be measured with an efficiency of about 0.5 and a contamination due to higher masses of about 0.02. On the contrary the iron spectrum can be measured with an efficiency of about 0.2 and with a contamination of about few percents.

References

[1] A. Fassò, A. Ferrari, J. Ranft, and P.R. Sala, CERN-2005-10 (2005), INFN/TC_05/11, SLAC-R-773
[2] S. M. Mari, F. Ronci, Proc. ICRC 2009, 1228.
[3] J. R. Hörandel, Astropart. Phys., 2003 **19**: 193